Investigation of Molecular Motions by Lee-Goldburg Cross-Polarization NMR Spectroscopy

Mei Hong,*,† Xiaolan Yao,† Karen Jakes,‡ and Daniel Huster†,§

Department of Chemistry, Iowa State University, Ames, Iowa 50011, and Department of Physiology and Biophysics, Albert Einstein College of Medicine, 1300 Morris Park Avenue, Bronx, New York 10461

Received: December 10, 2001; In Final Form: March 27, 2002

We demonstrate the use of Lee−Goldburg cross-polarization (LG-CP) NMR under fast magic-angle spinning (MAS) to investigate the amplitude and geometry of segmental motions in biomolecular and polymeric solids. Motional geometry information was previously available only from ^{2}H NMR, which, however, has limited site resolution and requires site-specific isotopic labeling. Using a 2D LG-CP technique, we resolve the ^{13}C−^{1}H or ^{15}N−^{1}H dipolar couplings according to the ^{13}C or ^{15}N isotropic chemical shift. Applications to systems undergoing 180° phenylene ring flips show spectral line shapes reflecting the geometry of the motion. Using this LG-CP technique, we measured the ^{13}C−^{1}H and ^{15}N−^{1}H dipolar couplings in the water-soluble and membrane-bound states of the colicin Ia channel domain. The backbone motions of the membrane-bound colicin scale both the Cα−Hα and N−H couplings similarly, thus ruling out rotation of the α-helices around their axes as a specific mechanism of motion. We also show that the sensitivity of the LG-CP spectra can be enhanced by the addition of a phase-inverted ^{1}H−^{13}C cross-polarization step, and the site resolution of the ^{15}N−^{1}H LG-CP spectra can be enhanced by ^{13}C indirect detection.

1. Introduction

Molecular dynamics is ubiquitous and plays an important role in the function of proteins, nucleic acids, synthetic polymers, and other macromolecules.[1] Nuclear magnetic resonance (NMR) spectroscopy is a powerful tool for investigating the detailed local motions in molecules. Traditionally, NMR spectroscopy yields dynamics information from relaxation time measurements and from ^{2}H line shape analysis.[2] The latter is particularly sensitive to the amplitude, geometry, and time scales of motions. However, ^{2}H NMR has drawbacks. For synthetic polymers, ^{2}H isotopic labeling is demanding. For proteins, ^{2}H NMR typically does not provide appropriate site resolution to be suitable for multiply labeled samples. To extract dynamic amplitudes with site resolution, one can alternatively employ two-dimensional (2D) magic-angle spinning (MAS) NMR. One of the simplest techniques is the 2D wide-line-separation experiment,[3,4] which yields the ^{1}H−^{1}H dipolar couplings in the indirect dimension, separated by the ^{13}C chemical shift of individual sites in the direct dimension. Another common experiment is DIPSHIFT,[5−7] which measures the heteronuclear dipolar coupling between a ^{1}H spin and a heteronuclear spin *S*. The dipolar couplings of different sites are separated according to the *S*-spin isotropic chemical shift. We have recently used the ^{13}C−^{1}H DIPSHIFT experiment to characterize the differential amplitudes of internal motions between the water-soluble and membrane-bound states of a bactericidal protein, the colicin Ia channel domain.[8]

While the DIPSHIFT experiment provides information on the motional amplitude, it typically does not yield the detailed geometry of motion.[7,9] This limited information content results from the fact that the dipolar time data are sampled within a rotation period, symmetric with respect to the center of the rotor period. Fourier transformation of the time-domain data yields only a broad envelope of the dipolar coupling pattern. This also means that the DIPSHIFT experiment cannot be applied at high spinning speeds, which are increasingly important for studies of multiply labeled proteins at high magnetic fields.

Recently, a Lee−Goldburg [10] cross-polarization (CP) experiment under fast magic-angle spinning was analyzed as a new tool for measuring heteronuclear dipolar couplings.[11,12] In this experiment, ^{1}H−*S* CP is established using a tilted spin-lock on the ^{1}H channel. The ^{1}H frequency offset during the spin-lock is related to the ^{1}H rf field strength by tan 54.7°, so that the effective field of the ^{1}H spins, ω_{eff}, is tilted from the *z*-axis by the magic angle, 54.7°. Under this condition, the ^{1}H−^{1}H homonuclear dipolar interaction is effectively suppressed. At the same time, if the ^{1}H effective field strength, $\omega_{\text{eff}} = \gamma_H B_{1\text{eff}}$, is matched to the *S*-spin spin-lock field strength, $\omega_{1S} = \gamma_S B_{1S}$, by $\omega_{\text{eff}} - \omega_{1S} = \pm\omega_r$, then the ^{1}H−*S* heteronuclear dipolar interaction is maintained and scaled by sin 54.7°. By incrementing the LG-CP contact time, the dipolar coupling between the ^{1}H and *S* spins can be measured in the indirect dimension and resolved according to the *S*-spin isotropic shifts in the direct dimension. Importantly, the LG-CP experiment is conducted rotor asynchronously and can use long evolution times; thus, the resulting dipolar spectra have higher accuracy than the DIPSHIFT spectra. The LG-CP spectral resolution is further enhanced by the fact that the averaged heteronuclear dipolar Hamiltonian is "γ-encoded"[13,14] and is thus less dependent on powder orientation angles.

In this paper, we show that the LG-CP experiment can be used to provide information on the amplitude and geometry of fast segmental motions. We extend the previous analysis of LG-CP heteronuclear dipolar couplings to the case where the

* To whom correspondence should be addressed: Department of Chemistry, Gilman 0108, Iowa State University, Ames, IA 50011. Tel: 515-294-3521. Fax: 515-294-0105. E-mail: mhong@iastate.edu.

† Iowa State University.

‡ Albert Einstein College of Medicine.

§ Current address: University of Leipzig, Institute of Medical Physics and Biophysics, Liebigstr. 27, 04103 Leipzig, Germany.

10.1021/jp0156064 CCC: $22.00 © 2002 American Chemical Society
Published on Web 06/28/2002

asymmetry parameter, η, of the dipolar tensor is no longer 0, due to anisotropic molecular motions. The LG-CP spectra of such nonuniaxially averaged dipolar interactions will exhibit line shapes indicative of both the amplitude and geometry of the motion. We demonstrate such nonuniaxial LG-CP dipolar spectra on a small amino acid, phenylalanine, and on an amorphous polymer, polycarbonate. We then show the use of LG-CP to exclude certain types of motional geometry in membrane-bound colicin Ia channel domain. Next, we present a simple modification of the original LG-CP experiment that increases the sensitivity by up to a factor of 2. Finally, we show that a ^{13}C-detected ^{15}N LG-CP experiment can be implemented to measure N−H dipolar couplings in peptides and proteins with enhanced site resolution.

2. Experimental Section

Materials. The unlabeled phenylalanine sample was obtained from Sigma. Bisphenol A-polycarbonate was kindly provided by Prof. Schmidt-Rohr. The pellets were melt-pressed into a glassy cylinder of 2.9-mm diameter and were fit snuggly into a 4 mm MAS rotor. ^{15}N-labeled *N*-acetylvaline was synthesized as described previously.[15] U-^{13}C,^{15}N-labeled glutamine was purchased from Cambridge Isotope Laboratory (Andover, MA) and used without further purification.

Colicin Ia channel domain was expressed from pKSJ120-containing *Escherichia coli* BL21 (DE3) and purified as described recently.[8] Cells were first grown overnight at 37 °C in 100 mL of a modified M9 medium containing, per liter, 1 g of NH_4Cl; 4 g of glycerol; 3 g of KH_2PO_4; 6 g of Na_2HPO_4; 0.5 g of NaCl; 15 mg of $CaCl_2$; 1 mM $MgSO_4$; the unlabeled amino acids Asp, Asn, Arg, Gln, Ile, Lys, Met, Pro, Thr, and Glu at 150 μg/mL each; and 100 μg/mL ampicillin. The cells were pelleted and resuspended in 10 mL of the same medium, but containing, per liter, 1.5 g of $^{15}NH_4Cl$, 150 μg/mL ^{15}N-labeled Glu, and 4 g of U-^{13}C-labeled glucose. These cells were used to inoculate 1 L of the stable-isotope-containing medium. The culture was grown to $OD_{660} = 0.4$ and then induced with 1 mM isopropyl β-D-thiogalactopyranoside. Cells were harvested after 3 h of induction at 37 °C. Soluble His-tagged colicin Ia channel domain was purified on His-Bind metal chelation resin (Novagen, Madison, WI). Approximately 30 mg of pure soluble protein was obtained from 1 L of culture. The purified protein eluted from the His-Bind resin in 1 M imidazole buffer was dialyzed extensively against distilled water and lyophilized. We call this sample partial−uniformly labeled colicin, to designate the fact that 10 out of 20 amino acids are labeled in ^{13}C,[16] but that the 10 labeled amino acids are uniformly labeled in ^{13}C. All the 10 amino acids from the glycolysis pathway, as well as glutamate, are uniformly labeled in ^{15}N.

To prepare the soluble colicin sample, the purified dry colicin powder was packed into a 4-mm NMR rotor and hydrated to 30% water by weight. For the membrane-bound sample, a protein−lipid molar ratio of 1:100 was used, and the lipids consisted of POPC and POPG at a molar ratio of 3:1. About half of the POPC was perdeuterated (d_{31}) in the *sn*-1 chain to enable assessment of the effect of colicin binding to lipid chain order. Unilamellar lipid vesicles were formed by extrusion through a 100-nm filter membrane. The aqueous solution of protein and lipids was ultracentrifuged at 150000*g*, and the resulting membrane pellet was lyophilized and rehydrated to a final water content of 30 wt %. Both the soluble and membrane-bound colicin samples were maintained at pH 4.8 in a citrate buffer (10 mM KCl and 10 mM citrate).

NMR Spectroscopy. All NMR experiments were carried out on a BRUKER DSX-400 spectrometer (Karlsruhe, Germany) operating at a resonance frequency of 400.49 MHz for ^{1}H, 100.72 MHz for ^{13}C, and 40.59 MHz for ^{15}N. A triple-resonance MAS probe with a 4-mm spinning module was used. The ^{1}H radio frequency (rf) field strength for heteronuclear TPPM decoupling [17] was 80 kHz. Carbon and nitrogen 90° pulses were typically 5.0 and 6.0 μs long, respectively. Cross-polarization contact time was typically 0.5 ms when it was not incremented as the evolution time of a 2D experiment. For the LG-CP period, the ^{1}H effective field strength was 50 kHz in all experiments, and the ^{13}C or ^{15}N spin-lock field strengths were usually adjusted to the first-order sideband condition $\omega_{1S} = \omega_{\text{eff}} - \omega_r$. Spinning speeds were typically 12−13 kHz and were regulated to ±3 Hz by a pneumatic control unit. Recycle delays varied from 1.5 s for proteins to 4 s for phenylalanine.

The 2D LG-CP experiments typically incremented the LG-CP contact time at a step of 10 or 15 μs. An exception was the ^{13}C-detected ^{15}N−^{1}H LG-CP experiment, which required the evolution period to be half-integer multiples of the rotation period. At a spinning speed of 13 kHz, the dwell time for the evolution period was thus 38.46 μs. The maximum t_1 evolution time was typically about 2 ms. Only cosine-modulated data were collected. Thus, a real Fourier transformation was performed on the t_1 data, yielding spectra with a symmetrized ω_1 dimension and showing the dipolar splittings. Since the t_1 time signal increases with increasing LG-CP contact time, the ω_1 dimension was processed using the baseline correction mode "qfil" in the XWINNMR software. This subtracts a constant intensity from the time signals before Fourier transformation and yields spectra free of a dominant zero-frequency peak.

For labeled glutamine and *N*-acetylvaline, only eight scans were coadded for each t_1 point of the 2D LG-CP experiment. For the ^{13}C−^{1}H LG-CP spectra of unlabeled phenylalanine and polycarbonate, 64−96 scans were added for each t_1 point. The colicin spectra required between 64 and 128 scans for the ^{13}C−^{1}H LG-CP experiment, and 320 scans for the ^{15}N−^{1}H LG-CP experiment.

3. Theory

LG-CP Line Shape of Nonuniaxially Averaged Dipolar Interactions. The theory of LG-CP under magic-angle spinning has been described recently.[11] Here, we will only present an analysis of the effect of fast motion on the line shape of the LG-CP spectra. In contrast to rigid-limit spin-pair couplings, the motionally averaged dipolar couplings can be nonuniaxial ($\bar{\eta} \neq 0$). We also describe the sensitivity-enhanced LG-CP experiment and the triple-resonance adaptation of the original double-resonance LG-CP experiment for indirect detection of the dipolar couplings.

Figure 1a shows the pulse sequence of the 2D LG-CP experiment under MAS. After two ^{1}H pulses that put the ^{1}H magnetization along the magic-angle direction alternately in the $+x/+z$ quadrant and the $-x/-z$ quadrant of the xz plane, a ^{1}H Lee−Goldburg spin-lock is applied simultaneously with a transverse ^{13}C spin-lock pulse. The ^{1}H effective field strength, ω_{eff}, is matched to the *S* spin-lock field strength ω_{1S}, by $\omega_{\text{eff}} - \omega_{1S} = \pm\omega_r$. The CP contact time is incremented asynchronously with rotation to yield the heteronuclear dipolar dimension of the 2D experiment. The *S*-spin isotropic chemical shift is detected in the second dimension of the experiment.

The $I-S$ dipolar interaction under the LG-CP irradiation, H_{IS}, is calculated in a doubly tilted rotating frame, whose z-axis is defined by the ^{1}H (I spin) and *S*-spin spin-lock

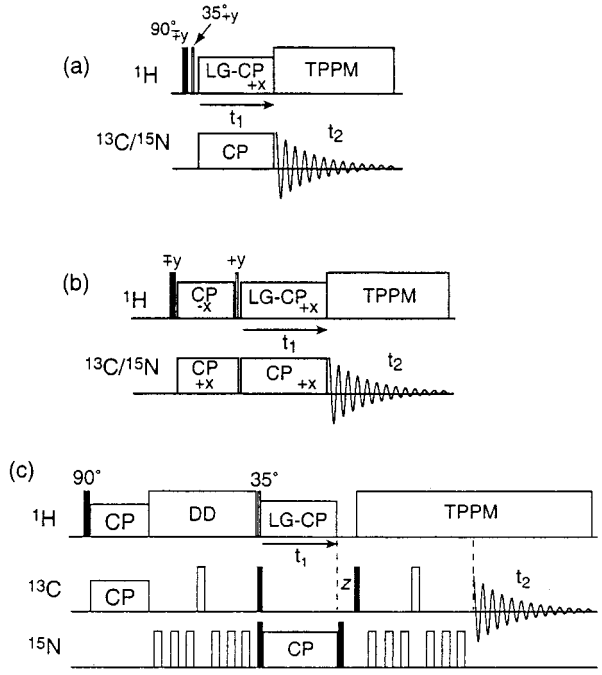

Figure 1. Pulse sequences used in this work: (a) 2D LG-CP under MAS, (b) 2D PILGRIM, with an additional phase-inverted HH-CP step before the LG-CP; (c) 2D ^{13}C -detected ^{15}N−^{1}H LG-CP.

fields. The Hamiltonian is

$$H_{IS}(t) = b(t)(I_z S_x \cos\theta_m - I_x S_x \sin\theta_m) \quad (1)$$

[11] where θ_m is the magic angle between the ^{1}H spin-lock field and the static magnetic field. The time-dependent dipolar coupling between I and S spins, $b(t)$, is

$$b(t) = 2\overline{\delta_d}(C_1\cos(\omega_r t + \gamma) + S_1 \sin(\omega_r t + \gamma) + C_2\cos(2\omega_r t + 2\gamma) + S_2 \sin(2\omega_r t + 2\gamma)) \quad (2)$$

The coefficients C_1, C_2, S_1, and S_2 depend on the asymmetry parameter, $\bar{\eta}$, of the motionally averaged dipolar tensor, and on the powder angles, (α, β, γ), that describe the relative orientation of the rotor frame with the principal axis system of the averaged dipolar tensor.[18] The dipolar coupling constant, $\overline{\delta_d}$, represents the motionally averaged coupling.

Since the rf Hamiltonian in the doubly tilted frames, $H_{rf} = \omega_{eff} I_z + \omega_{1S} S_z$, is significantly stronger than the heteronuclear dipolar coupling, H_{IS} is averaged to only components that commute with H_{rf}. This averaged dipolar interaction is calculated by transformation to an interaction frame defined by the rf pulses according to $H_{IS}^* = \exp(iH_{rf}t)H_{IS}\exp(-iH_{rf}t)$.[19] In this interaction frame, under the condition $\omega_{1S} = \omega_{eff} \pm \omega_r$, the time-dependent terms in the dipolar Hamiltonian are averaged, leaving only the time-independent part:

$$\overline{H_{IS}^*} = \frac{1}{2}\overline{\delta_d}\sin\theta_m[I_x^{(23)}(C_1\cos\gamma + S_1\sin\gamma) - I_y^{(23)}(C_1\sin\gamma - S_1\cos\gamma)] \quad (3)$$

The zero-quantum two-spin operators, $I_{x,y,z}^{(23)}$, are defined as

$$I_x^{(23)} = I_x S_x + I_y S_y \qquad I_y^{(23)} = I_y S_x - I_x S_y \qquad I_z^{(23)} = \frac{1}{2}(I_z - S_z) \quad (4)$$

The average Hamiltonian in eq 3 can be rewritten as

$$\overline{H_{IS}^*} = \frac{1}{2}\overline{\delta_d}\sin\theta_m(I_x^{(23)}, I_y^{(23)}, I_z^{(23)}) = \frac{1}{2}\overline{\delta_d}\sin\theta_m\sqrt{C_1^2 + S_1^2}\cdot\overrightarrow{I^{(23)}}\cdot\overrightarrow{B_{IS,LG}}\begin{pmatrix} C_1\cos\gamma + S_1\sin\gamma \\ C_1\sin\gamma - S_1\cos\gamma \\ 0 \end{pmatrix} \quad (5)$$

This shows that the averaged dipolar interaction is analogous to the Zeeman interaction in that it is a scalar product between a spin operator, $\overrightarrow{I^{(23)}}$, and an effective magnetic field, $\overrightarrow{B_{IS,LG}}$ with unit length. The strength of the interaction depends on both C_1 and S_1.

The effect of the zero-quantum heteronuclear dipolar Hamiltonian on the magnetization is calculated using the von-Neumann equation. The density operator at the beginning of the LG-CP period, expressed in the doubly tilted frame, is

$$\rho(0) = I_z = I_z^{(14)} + I_z^{(23)} \quad (6)$$

where $I_z^{(14)} = (I_z + S_z)/2$. The $I_z^{(23)}$ term precesses around $\overrightarrow{B_{IS,LG}}$ in the zero-quantum spin space, while the $I_z^{(14)}$ term is stationary. This yields the following observable magnetization terms:

$$\rho_{obs}(t) = \frac{1}{2}I_z(1 + \cos\omega_{IS,LG}t) + \frac{1}{2}S_z(1 - \cos\omega_{IS,LG}t). \quad (7)$$

Of these, only the S-spin term is detected in the experiment. The dipolar oscillation frequency $\omega_{IS,LG}$ follows eq 5 and is given by

$$\omega_{IS,LG} = \frac{1}{2}\overline{\delta_d}\sin\theta_m\sqrt{C_1^2 + S_1^2} \quad (8)$$

where $C_1 = -\sqrt{2}/2\sin 2\beta(1 + \bar{\eta}\cos 2\alpha/3)$ and $S_1 = -\sqrt{2}/3\bar{\eta}\sin\beta\sin 2\alpha$. Since both C_1 and S_1 depend on $\bar{\eta}$, the heteronuclear dipolar coupling frequency also depends on $\bar{\eta}$.

Sensitivity-Enhanced LG-CP Spectroscopy. The sensitivity of the LG-CP spectra can be enhanced by preparing the initial state of the spins differently from the pulse sequence in Figure 1a. The modification is analogous to the PISEMA technique,[20,21] which is used under the nonspinning condition to measure heteronuclear dipolar interactions in oriented membrane peptides. In this modified LG-CP experiment (Figure 1b), a Hartman−Hahn CP (HH-CP) from ^{1}H to S spins is inserted prior to the LG spin-lock on ^{1}H. The ^{1}H spin-lock field direction relative to the ^{1}H magnetization is inverted between the first and the second CP steps. This phase-inverted HH-CP changes the density operator at the beginning of LG-CP to

$$\rho(0) = \epsilon(I_z - S_z) = 2\epsilon\cdot I_z^{(23)} \quad (9)$$

The factor ϵ is a number smaller than or equal to 1 and depends on the extent of magnetization equilibration as a result of ^{1}H spin diffusion (see below). Comparing the density operator in eq 9 with that of eq 6, we find the relevant zero-quantum coherence to be enhanced by a factor of 2ϵ. This zero-quantum coherence oscillates under the zero-quantum dipolar Hamiltonian with the same frequency as eq 8 and yields the following observable I and S magnetization:

$$\rho_{obs}(t) = \epsilon(I_z\cos\omega_{IS,LG}t - S_z\cos\omega_{IS,LG}t) \quad (10)$$

When comparing eqs 7 and 10, one must keep in mind that the constant of 1 in eq 7 for the *S*-spin magnetization under LG-CP does not contribute to the dipolar signal of interest, since this constant is subtracted before Fourier transformation. In other words, only the oscillatory part of the *S* magnetization affects the spectral intensity.

If spin diffusion among ^{1}H spins is efficient, an *S*-spin in thermal contact with n ^{1}H spins will obtain an *S*-magnetization of $\epsilon \approx n/(n+1)$. Therefore, this modified LG-CP experiment, which we shall call PILGRIM for *p*hase-*i*nverted *LG r*ecoupl*i*ng under *M*AS, enhances the oscillatory part of the *S*-spin signal by

$$2\epsilon \approx \frac{2n}{n+1} \tag{11}$$

compared to the original LG-CP experiment. In ^{13}C unlabeled compounds, where the number of ^{1}H spins (n) relative to each *S*-spin is large, and under slow to intermediate MAS spinning speeds (<10 kHz), when ^{1}H spin diffusion is efficient, $\epsilon \rightarrow 1$. Thus, a maximum enhancement factor of 2 can be expected from the PILGRIM experiment. However, for uniformly ^{13}C-labeled peptides, the ratio of ^{1}H to ^{13}C is much smaller, typically about 2−3 to 1, depending on whether the ^{13}C−^{1}H group is located in the backbone or the side chain and whether the side chain is a ^{1}H-rich aliphatic segment or a ^{1}H-poor aromatic ring. Moreover, higher spinning speeds reduce the efficiency of ^{1}H spin diffusion and further decrease the *S*-spin CP signal, as shown by Vega and co-workers using Floquet theory.[22] Thus, the enhancement factor is usually less than 2. It is important to note that the treatment given here is for an isolated $I-S$ spin pair, such as a C−H or N−H group, and does not take into account complex multiple-spin dynamics during LG-CP at long times. The $n-1$ protons in spin diffusion contact are considered during HH-CP but neglected during the LG-CP period due to truncation by the strongest C−H dipolar coupling.[23]

^{13}C-Indirectly Detected ^{15}N−^{1}H LG-CP Experiment. For applications to proteins, it is sometimes of interest to extend the double-resonance LG-CP experiment to a triple-resonance experiment. For example, it will be useful to measure the N−H dipolar couplings with ^{13}C detection, since the site resolution of the Cα region of the protein spectra is usually better than the resolution of the ^{15}N spectra. Figure 1c shows one way of implementing this ^{13}C-detected ^{15}N−^{1}H LG-CP experiment. The ^{13}C−^{15}N polarization transfer is accomplished by a REDOR sequence in a heteronuclear single-quantum coherence (HSQC) [24] fashion. The spin operator at the beginning of the ^{15}N−^{1}H LG-CP evolution period, after the first train of REDOR pulses, can be represented by C_zN_x. Since the magnetization does not reside on the ^{1}H spins, the evolution of the spin operator under the LG-CP Hamiltonian differs from the previous two experiments in that the ^{15}N magnetization decreases, rather than increases, with increasing CP contact time. But the oscillation frequency is still identical to eq 8.

After the evolution period, the ^{15}N transverse magnetization is returned to the *z*-axis by a ^{15}N 90° pulse. After a variable *z*-filter (see below), a ^{13}C 90° pulse generates the transverse ^{13}C coherence that is antiphase with ^{15}N. This evolves under a second REDOR period to create the in-phase ^{13}C magnetization, which is detected during t_2.

The first and second REDOR periods must be rotor-synchronized in the experiment. This requires that the LG-CP evolution time be synchronized with sample rotation. To ensure sufficient spectral width for the dipolar dimension, we used half a rotor period as the dwell time for the evolution period and chose the *z*-filter to be half a rotor period for those evolution times that are odd integer multiples of the dwell time.

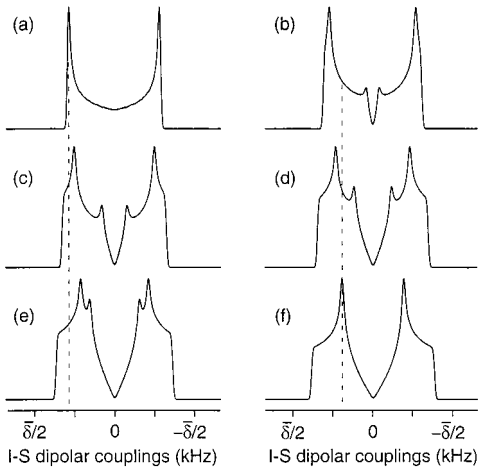

Figure 2. Simulated LG-CP dipolar spectra for motions with varying asymmetry parameter $\bar{\eta}$: (a) 0, (b) 0.2, (c) 0.4, (d) 0.6, (e) 0.8, (f) 1.

Line Shape Simulations. The $\bar{\eta}$-dependent LG-CP spectral line shapes were simulated in the frequency domain according to eq 8. The two-site 180° phenylene ring flip motion has a well-defined average dipolar coupling constant of $\bar{\delta}_d = \delta_d(3 \sin^2 \beta_r/2 - 1)/2$, where β_r is the reorientation angle of the C−H bonds off the flip axis before and after the motion and is close to 120°. δ_d is the rigid-limit one-bond C−H dipolar coupling constant, which is 22.7 kHz. The asymmetry parameter of the averaged tensor can be calculated as

$$\eta = \frac{3\cos^2(\beta_r/2)}{3\sin^2(\beta_r/2) - 1}$$

The motions in glassy polycarbonate were simulated by considering a two-site phenylene ring flip combined with wobbling of the aromatic ring around the equilibrium positions. The wobbling angle is modeled using a Gaussian distribution with a width of σ. This width itself is distributed due to the amorphous nature of this glassy polymer[7,25] (see below).

4. Results and Discussion

Geometry of Motion Detected by LG-CP. Figure 2 shows the calculated LG-CP line shapes for asymmetry parameters ranging from 0 to 1 at an increment of 0.2. For a uniaxial motionally averaged interaction with $\bar{\eta} = 0$, the spectrum (Figure 2a) resembles a Pake pattern without the outer two "shoulders". The splitting is 0.57 times ($\cos \theta_m$) the motionally averaged coupling $\bar{\delta}_d$. As $\bar{\eta}$ increases, both the intensity at the center of the spectrum and the splitting between the two maxima decrease. At the maximum $\bar{\eta}$ of 1, the dipolar splitting equals $0.39\bar{\delta}_d$, and two distinct outer shoulders can be seen in the spectrum.

Figure 3 shows the ^{13}C−^{1}H LG-CP spectra of the amino acid phenylalanine. The aromatic ring in phenylalanine undergoes 180° flips on a time scale that is fast compared to the C−H dipolar interaction. Since the motionally averaged tensors for this two-site ring flip motion can be calculated readily, phenylalanine serves as a good model system to test the use of LG-CP to provide information on the geometry of motion.

It is known that phenylalanine can crystallize into different structures depending on the solvents used.[26] The different molecules exhibit different ring dynamics, and spectral editing

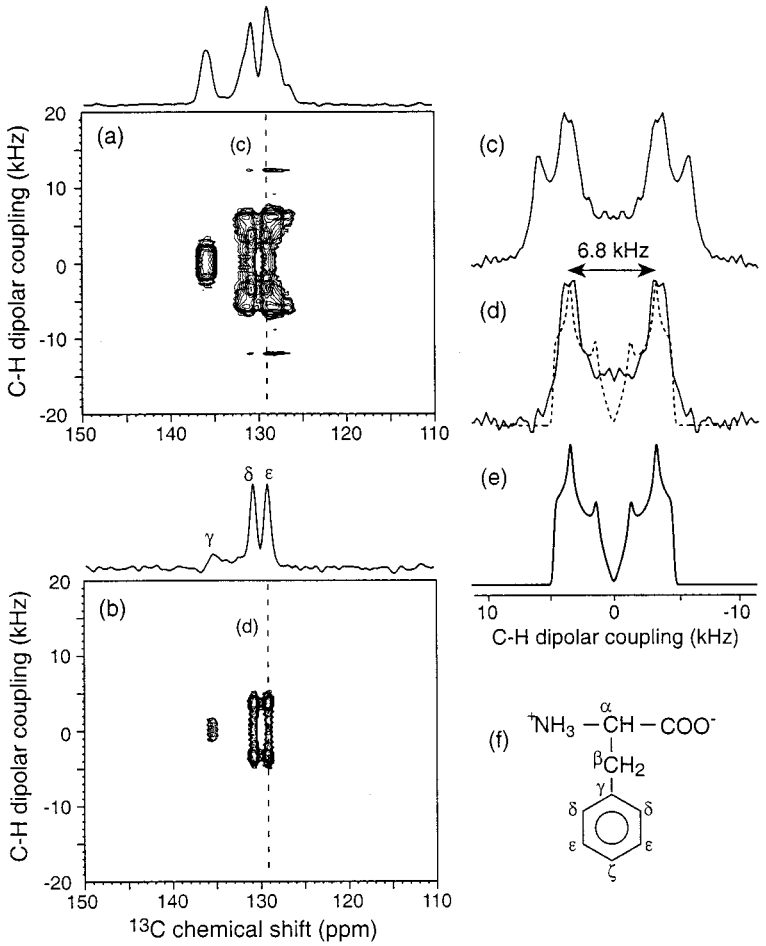

Figure 3. ^{13}C−^{1}H LG-CP spectra of Phe: (a) 2D LG-CP spectrum without a T_1 filter, (b) 2D LG-CP spectrum with an "inverse" T_1 filter that selects only sites with short ^{13}C T_1 values, (c) cross section at 129.1 ppm (Cϵ) from the unfiltered spectrum a, (d) corresponding cross section from the T_1-filtered spectrum, (e) best-fit simulation, with $\bar{\eta} = 0.5$ and $\delta_d = 14.2$ kHz. (f) Nomenclature and molecular structure of Phe.

is necessary to select for molecules with the expected ring-flip motion. For samples crystallized from water, it was found previously that the aromatic region of the ^{13}C spectrum shows two types of peaks with different ^{13}C spin−lattice relaxation times (T_1). Only the molecules with short T_1 values give rise to ^{2}H spectra expected for the two-site ring flip motion.[26] To select for the ^{13}C signals with short T_1 times, we applied a ^{13}C T_1 filter after the C−H LG-CP evolution period.[27] The reference spectrum (Figure 3a) was obtained using a short *z*-filter of 1 ms, so that all ^{13}C signals are retained. The dipolar cross section at the Cϵ cross section (Figure 3c) shows two splittings. A dephased spectrum, acquired with a *z*-filter of 1.5 s, suppressed the ^{13}C intensities from molecules with T_1 shorter than 1.5 s, while retaining those signals with longer T_1. The difference between the reference and the dephased spectra[27] yielded the 2D LG-CP spectrum (Figure 3b) of sites with short T_1 times. As can be seen, the Cδ and Cϵ peaks are significantly narrowed in the chemical shift dimension by the subtraction procedure. The LG-CP line shape of the Cϵ cross section after this inverse T_1 filter is shown in Figure 3d. A splitting of 6.8 kHz is observed, and the line shape is distinctly neither $\bar{\eta} = 0$ nor $\bar{\eta} = 1$. Best-fit simulation (Figure 3e) yielded an $\bar{\eta}$ of 0.5 for the motionally averaged dipolar tensor. Compared to the simulation, the experimental spectrum is somewhat broadened and does not show an inner shoulder present in the simulated spectrum. This broadening may result from longer range C−H dipolar couplings that are not included in the two-spin calculation and from incomplete removal of the heterogeneity of the sample.

Analytical solutions for the motionally averaged C−H tensor under fast 180° ring flips shows that the three principal values of the averaged tensor are related to the reorientation angle β_r according to $\overline{\omega_1} = \delta_d[3\sin^2(\beta_r/2) - 1]/2$, $\overline{\omega_2} = \delta_d[3\cos^2(\beta_r/2) - 1]/2$, and $\overline{\omega_3} = -\delta_d/2$.[18] If the C−H bond of δ and ϵ sites is perfectly 60° from the flip axis Cγ−Cζ (Figure 3f), then the reorientation angle β_r should be 120°. This results in an asymmetry parameter of 0.6 for the motionally averaged dipolar tensor. Our experimentally determined $\bar{\eta}$ of 0.5 deviates from the ideal value and may be accounted for by a small deviation of the reorientation angle from 120°. Indeed, a reorientation angle of 123.7° yields an $\bar{\eta}$ of 0.5. Thus, the δ and ϵ C−H bonds may deviate from the ideal hexagonal symmetry by less than 2°.

A more complex example of motion involving 180° ring flip is found in polycarbonate, where the two phenylene rings in each monomer unit undergo 180° flips superimposed with wobbling motions with a distribution of amplitudes around the equilibrium positions.[7,25] Figure 4 shows the 2D ^{13}C−^{1}H LG-CP spectrum of polycarbonate and several cross sections. A ^{13}C 1D LG-CP MAS spectrum is shown at the top of the 2D spectrum, where the five resolved ^{13}C signals are assigned on the basis of the literature.[9] The C−H cross section of signal 4, which results from the aliphatic quaternary carbon, is shown in Figure 4b. It does not exhibit any resolved splitting, as expected for a carbon site that is not directly bonded to any protons. In comparison, the aromatic carbon 3 off the flip axis exhibits a splitting of 6.6 kHz and a smooth line shape devoid of sharp

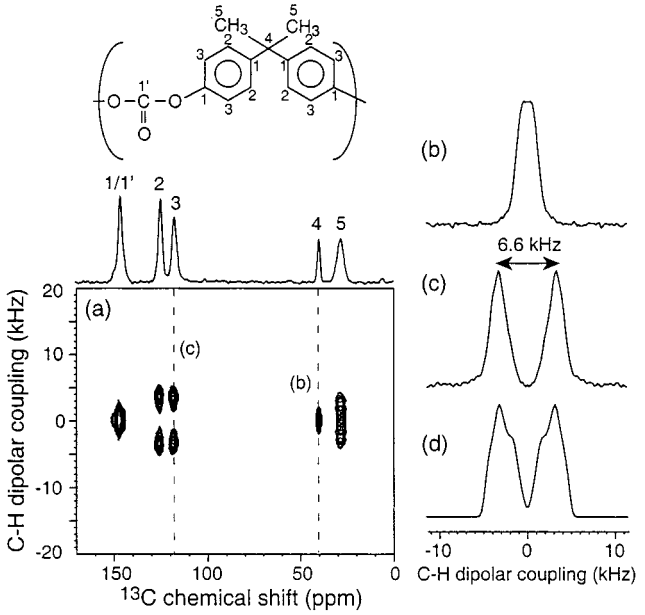

Figure 4. 2D ^{13}C−^{1}H LG-CP spectrum of polycarbonate: (a) 2D spectrum; the ^{13}C projection is shown at the top; (b) cross section of the quaternary carbon 4; (c) cross section of the aromatic carbon 3; (d) best-fit simulation for spectrum c, obtained with a reorientation angle of 120° and a wobbling amplitude distribution Σ of 20°.

features. To fit this spectrum, we use the model that the aromatic rings both undergo 180° flips and wobble around the equilibrium ring positions with an amplitude of σ. This motional model was previously deduced from ^{2}H and ^{13}C NMR experiments [9,25,28]. Assuming that the wobbling angle distribution is Gaussian, then the dipolar coupling is averaged from the C−H coupling frequency of a flipping phenylene ring, $\omega_{IS,LG}^{flip}$, according to

$$\overline{\omega(\sigma)} = \int d\phi\, \omega_{IS,LG}^{flip}(\phi) \frac{\exp(-\phi^2/2\sigma^2)}{(2\pi\sigma)^{1/2}} \qquad (12)$$

For a given wobbling amplitude, σ, a powder spectrum $S_\sigma(\omega)$ characterized by $\overline{\delta_\sigma}$ *and* $\overline{\eta_\sigma}$ can be obtained. Due to the amorphous nature of polycarbonate, the wobbling amplitude σ varies for different rings. If we represent this distribution by another Gaussian function $P_\Sigma(\sigma)$, then the final spectrum is a superposition of subspectra for various wobbling amplitudes:

$$S(\omega,\Sigma) = \int d\sigma\, S_\sigma(\omega)\, P_\Sigma(\sigma) \qquad (13)$$

We found that a Gaussian distribution with $\Sigma = 20°$, combined with a 180° flip with a C−H reorientation angle of 120°, resulted in a reasonable fit, as shown in Figure 4d. These angles also yielded a simulated ^{2}H spectral line shape (not shown), in good agreement with the previously observed ^{2}H spectra.[7,25]

Dynamics in the Colicin Ia Channel Domain through N−H and C−H Dipolar Couplings. The colicin Ia channel-forming domain inserts spontaneously into lipid bilayers from an aqueous environment to carry out its bactericidal function.[29] We have recently shown that the protein in the membrane-bound state executes larger amplitude internal motions than in its water-soluble state.[8] This was manifested in the narrowed ^{1}H wide-line spectra and the reduced C−H DIPSHIFT dephasing curves. Moreover, the side chains increase their motional amplitudes more strongly than the backbone in the membrane-bound state.

To determine the geometry of backbone motions in the membrane-bound colicin, we set out to compare the N−H

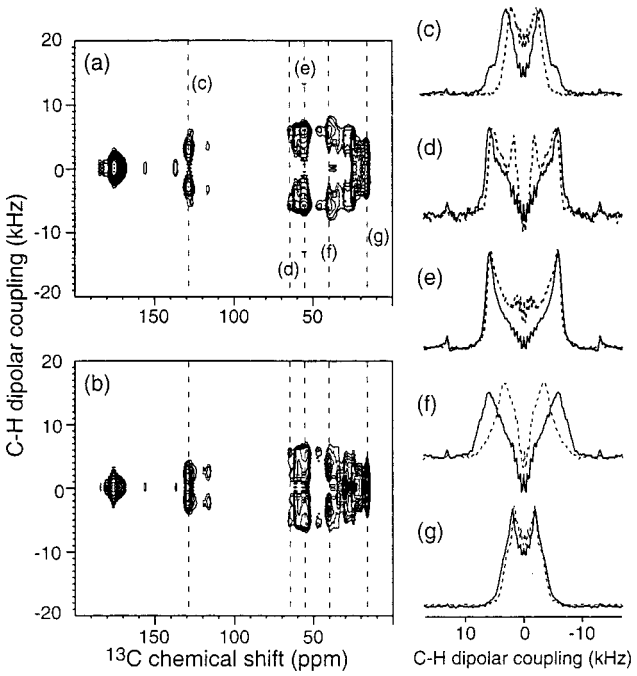

Figure 5. ^{13}C−^{1}H LG-CP spectra of colicin Ia channel domain: (a) 2D spectrum of the soluble colicin. (b) 2D spectrum of the membrane-bound colicin. Various cross sections are extracted from each 2D spectrum. Solid and dotted lines represent the soluble and membrane-bound colicin, respectively. (c) Cross section at 128.6 ppm for Phe Cδ. (d) Cross section at 64.5 ppm for Val Cα. (e) Cross section at 54.8 ppm for Ala Cα. (f) Cross section at 40 ppm for Leu Cβ (CH_2 group). (g) Cross section at 16 ppm for Ala Cβ (CH_3 group).

dipolar couplings between the two states of the protein using the LG-CP technique. Since the protein is about 80% helical[30] and the N−H bonds in α-helices are roughly parallel to the helical axis, the N−H dipolar coupling will indicate whether the backbone motion is a reorientation around the individual helix axis. Reorientation around the helix axis in the membrane will not affect the N−H dipolar coupling, so that the membrane-bound and water-soluble colicins should both exhibit the same N−H dipolar couplings. In contrast, any other backbone motion of the membrane-bound colicin would reduce the N−H dipolar couplings for the membrane-bound sample more than for the soluble colicin.

We first confirmed the previous C−H dipolar dephasing results by measuring the C−H LG-CP spectra of the water-soluble and membrane-bound colicin. These samples are uniformly ^{13}C- and ^{15}N-labeled in the 10 amino acids produced from the glycolysis pathway (His, Ala, Leu, Val, Ser, Gly, Cys, Phe, Tyr, Trp). In addition, ^{15}N-labeled Glu was added to the expression media to reduce dilution of the ^{15}N labels in the 10 desired amino acids by the transamination reaction. Figure 5 shows the C−H LG-CP spectra of colicin. As expected, the carbonyl region shows no significant splitting, while the aromatic and aliphatic regions show well-resolved C−H dipolar splittings. The cross sections from 128.6 ppm (Phe Cδ), 64.5 ppm (Val Cα), 54.8 ppm (Ala Cα), 40 ppm (Leu Cβ), and 16 ppm (Ala Cβ) are shown. Clearly, the water-soluble colicin (solid lines) exhibits larger C−H dipolar splittings than the membrane-bound colicin (dashed lines) for most sites. This is particularly significant for the aromatic and aliphatic side chains, where the narrowing factors, $\bar{\delta}_{CH,mem}/\bar{\delta}_{CH,sol}$, for the C−H couplings are as small as 0.6. In comparison, the narrowing factors for the backbone Cα sites are much closer to 1, with the Ala Cα (54.8 ppm) showing a reduction factor of 0.97 and

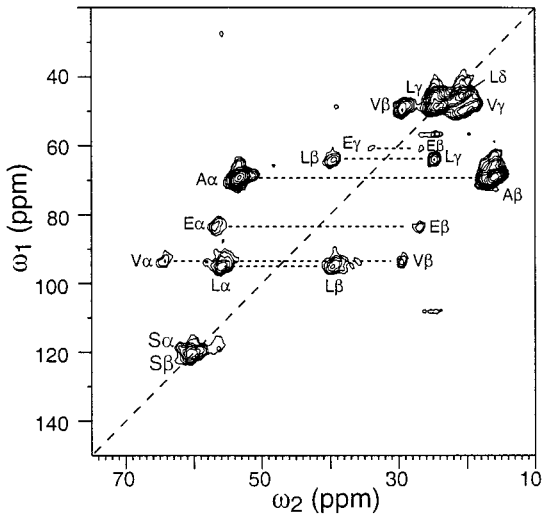

Figure 6. 2D ^{13}C double-quantum correlation spectrum of water-soluble colicin Ia channel domain. The spectrum was acquired under a spinning speed of 6.5 kHz. Amino acid type assignment for various peaks is indicated by single-letter codes. Note the overlapping Ser Cα and Cβ peaks along the slope-2 diagonal (dashed line) of the spectrum.

the Val Cα (64.5 ppm) exhibiting a narrowing factor of 0.95. These values are overall consistent with the results of the C−H DIPSHIFT dephasing experiments.[8]

Compared to the time-domain dephasing experiment, the LG-CP technique has the advantage of manifesting multiple couplings in a single cross section. For example, the Val Cα cross section for the membrane-bound protein exhibits a second splitting at 3.5 kHz, which is much smaller than the main coupling of 11.1 kHz. This indicates that certain Val residues undergo larger amplitude motions than the rest. While we cannot at present definitively assign this coupling to specific residues, we hypothesize that at least the Val in the N-terminal His tag used to purify the protein is responsible. ^{15}N single-pulse experiments (not shown) on the two colicin samples show that the His tag is nearly isotropically mobile in the membrane-bound state, since the resolved His side chain ^{15}N signal is much more intense in the membrane-bound colicin sample. In contrast, the DIPSHIFT dephasing experiment exhibits only the average of all couplings for each resolved site; thus, the presence of a small number of highly mobile residues biases the coupling results to smaller narrowing factors. This may explain the small difference in the quantitative value of the Val Cα narrowing factors between the previous DIPSHIFT experiment and the current LG-CP measurement.

The cross section at 60.5 ppm (Ser) also exhibits a secondary dipolar splitting (spectra not shown). The reduction factor for the larger splitting is 0.95 but 0.5 for the smaller splitting. We have acquired 2D $^{13}C-^{13}C$ double-quantum correlation spectra (Figure 6 below) that indicate that both the Ser Cα and Cβ peaks resonate at the same isotropic shift. Since all resolved side chains exhibit smaller C−H narrowing factors than the backbone sites, the Cβ−Hβ coupling of Ser most likely contributed to the small splitting in the same cross section as Ser Cα.

The Ala Cβ−Hβ coupling exhibits a small narrowing factor of 0.9 (Figure 5g) between the membrane-bound state and the water-soluble state, which is much larger than the Cβ narrowing factors of other residues such as Leu (0.6). This is due to the fact that the Ala methyl group already undergoes fast three-site jumps in the soluble state, and membrane binding cannot reduce the coupling further other than through the small-amplitude backbone motion.

The $^{13}C-^{13}C$ double-quantum correlation spectrum[31,32] of the water-soluble colicin Ia channel domain (Figure 6) confirms the amino acid type assignment used in analyzing the dipolar cross sections in the $^{13}C-^{1}H$ LG-CP spectra. The membrane-bound protein has a very similar 2D spectrum. The assignment of the overlapping Ser Cα and Cβ peaks is based on their overlapping frequencies on the slope-2 diagonal of the spectrum, as the two coupled spins in each ω_1 cross section must be centered around this diagonal.

Figure 7 shows the $^{15}N-^{1}H$ 2D LG-CP spectra of the two states of colicin. From the main ^{15}N cross section at 120 ppm, a splitting of 5.6 kHz is obtained for the soluble colicin and 5.4 kHz for the membrane-bound protein. This corresponds to a narrowing factor of 0.96, which is nearly identical to the average C−H narrowing factors obtained for the backbone Cα−Hα sites. This N−H coupling result is confirmed by a ^{13}C-detected $^{15}N-^{1}H$ LG-CP experiment on both samples (data not shown), which yielded similar N−H narrowing factors between the membrane-bound protein and the soluble protein. Furthermore, a $^{15}N-^{1}H$ DIPSHIFT experiment also indicated that the membrane-bound colicin has weaker N−H dipolar couplings than the soluble colicin.

The current understanding of the structure of the membrane-bound colicin states that most α-helices in the protein are located at the lipid−water interface, while a small fraction of residues, most likely a hydrophobic stretch designated as helices 8 and 9, are immersed in the hydrophobic core of the lipid bilayer. This overall topology has recently been confirmed by our 2D ^{1}H spin diffusion measurements.[33] Moreover, the helices at the lipid−water interface form an extended array, as evidenced by both fluorescence measurements [34] and our solid-state Cα chemical shift analysis.[35] On the basis of this structural model, one may envision that the helices in the plane of the bilayer undergo small-amplitude reorientation around the helical axes. Such helix reorientation has been detected in several other membrane proteins, such as rhodopsin and potassium channel proteins.[36,37] However, the present N−H dipolar coupling measurement, which shows reduced N−H couplings for the membrane-bound protein than the soluble protein, suggests that the additional motion in the membrane-bound colicin is not reorientation around the helical axis. Instead, the motion may be small-angle wobbling that affects all segments of each residue or helix rotation around axes different from the long axis, since the N−H narrowing factors are similar to the Cα−Hα narrowing factors. Such motions may simply be a result of collisions with the lipid molecules of the bilayer. The lack of reorientation around the long axis of the helix has the advantage that it preserves the favorable electrostatic interaction of the amphiphilic helices with the polar water and the nonpolar lipids at the lipid−water interface.

It is worth noting that the N−H coupling strengths for both the water-soluble and membrane-bound colicin are reduced from the rigid-limit N−H coupling expected for an amide group. Figure 8 shows the N−H LG-CP spectra for the amide N−H group of *N*-acetylvaline and for the side chain NH_2 group of glutamine. The former has a splitting of 6 kHz, while the latter has a more complex line shape due to the three-spin dynamics with a main splitting of 6.2 kHz. These indicate that the N−H dipolar couplings in the soluble and membrane-bound colicins have an order parameter of 0.93 and 0.9, respectively. This may reflect small-angle wobbling of individual residues or libration of the peptide planes that were detected by ^{2}H NMR.[38]

In addition to the main N−H coupling of 5.4 kHz, the membrane-bound colicin has a small population of sites with

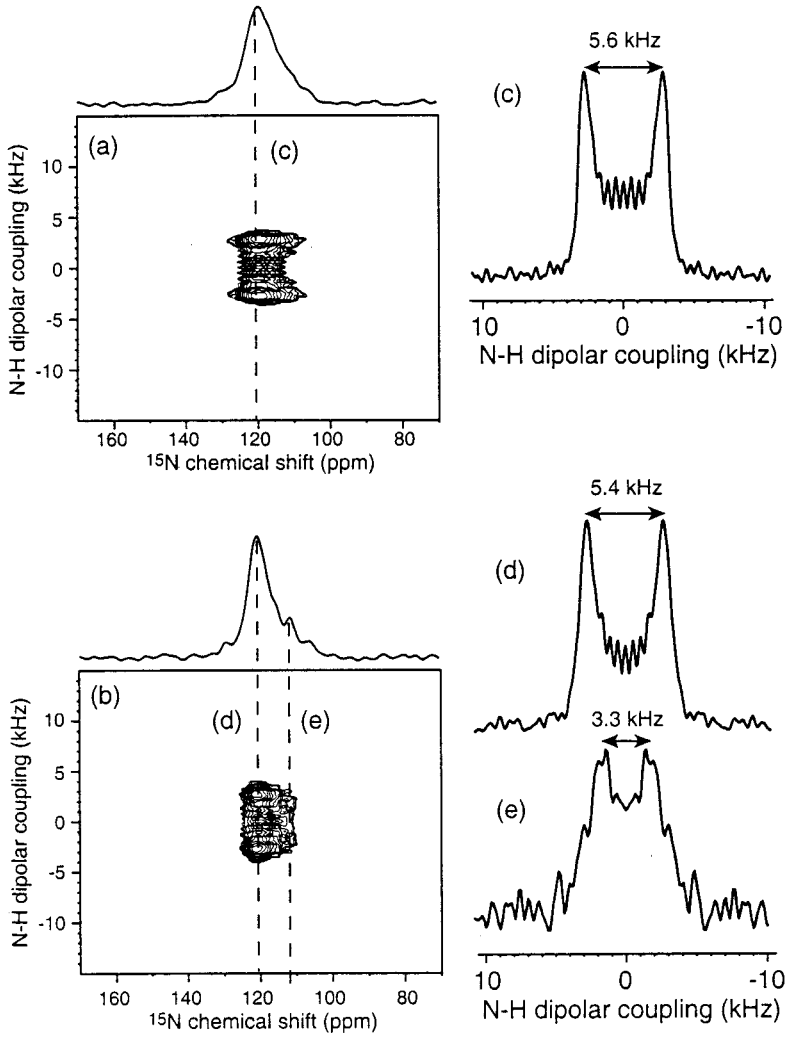

Figure 7. 2D ^{15}N $-^{1}$H LG-CP spectra of the colicin Ia channel domain in the water-soluble (a) and membrane-bound (b) states. The projection onto the ^{15}N dimension is shown at the top of each spectrum. (c) Cross section at 120 ppm from spectrum a. (d) Cross section at 120 ppm from spectrum b. (e) Cross section at 112 ppm from spectrum b.

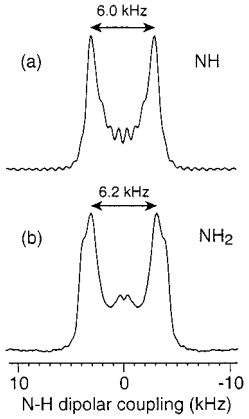

Figure 8. ^{15}N$-^{1}$H LG-CP spectra of rigid amino acids: (a) NH group of *N*-acetylvaline, (b) side chain NH_2 group of glutamine.

N−H couplings significantly attenuated to about 3.3 kHz (Figure 7e). This population has a ^{15}N isotropic shift of 112 ppm. Since Gly, His, and Ser residues have characteristically upfield ^{15}N chemical shifts, these sites with reduced N−H couplings most likely result from the highly dynamic His tag, which contains seven His residues, five Ser residues, and three Gly residues.

Sensitivity-Enhanced LG-CP Spectra by PILGRIM. Figure 9 shows the ^{13}C$-^{1}$H LG-CP spectrum of U-^{13}C,^{15}N-labeled glutamine obtained with the PILGRIM sequence (Figure 1b). The Cα, Cγ, and Cβ cross sections of the 2D spectrum (thick lines) are extracted and compared with the corresponding cross sections from the standard LG-CP experiment (thin lines) without the phase-inverted HH-CP step. The two experiments were otherwise conducted under the same conditions and with the same amount of signal averaging. It can be seen that the intensities of the PILGRIM spectra are generally higher than the corresponding LG-CP spectra. The enhancement factors for Cα, Cγ, and Cβ are 1.38, 1.36, and 1.53, respectively. For the C$\alpha-$Hα segment, the enhancement factor translates into an effective ^{1}H$-^{13}$C spin number ratio of 2.2, according to eq 11. This results from both reduced ^{1}H spin diffusion at the spinning speed of 13 kHz and the low number ^{1}H spins relative to ^{13}C spins in this uniformly labeled compound.

While both the Cβ and Cγ segments are methylene group whose enhancement factor cannot be predicted from eq 11 for $I-S$ spin pairs, the relative size of their enhancements is consistent with the number of ^{1}H spins in the local environment of β and γ segments. Namely, the β segment is adjacent to the γ methylene group and the α methine group, while the γ segment is located between a proton-poor carbonyl group and the β methylene group. Thus, the higher enhancement of the C$\beta-$Hβ coupling is to be expected. For the entire glutamine molecule, the total number of ^{1}H and ^{13}C spins is 10 and 5,

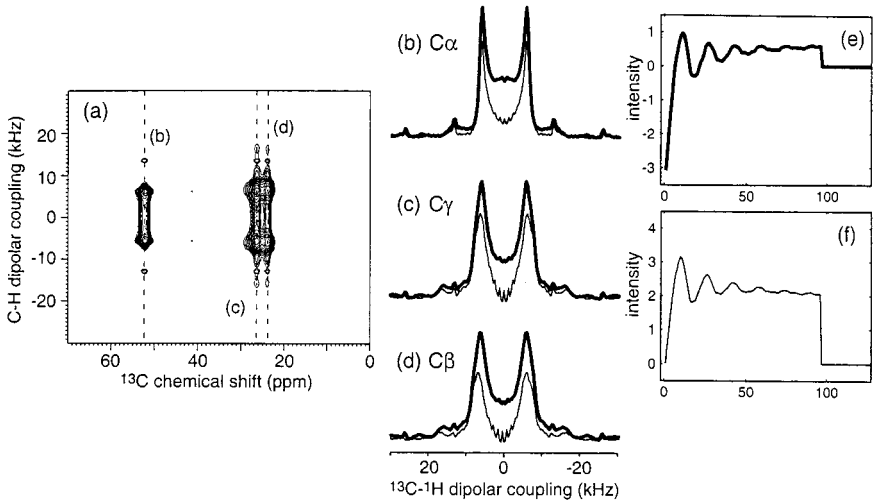

Figure 9. $^{13}C-^{1}H$ LG-CP dipolar patterns of glutamine Cα, Cβ, and Cγ sites, acquired by the PILGRIM technique (thick line) and by the simple LG-CP technique (thin line): (a) 2D PILGRIM spectrum of glutamine, (b) Cα cross section, (c) Cγ cross section, (d) Cβ cross section, (e) PILGRIM t_1 oscillation of C$\alpha-$Hα, (f) LG-CP t_1 oscillation of C$\alpha-$Hα. Intensities are drawn to scale for e and f.

respectively. Thus, the measured sensitivity enhancement is reasonable.

Parts e and f of Figure 9 show the time-domain oscillations of the PILGRIM and LG-CP experiment, respectively, for the C$\alpha-$Hα segment. Both curves appear as inverted free induction decays, as predicted by the negative sign in eqs 7 and 10. However, the PILGRIM time oscillation has an amplitude difference of about 3.5 between the initial value and the equilibrium value, while the LG-CP oscillation only has an amplitude change of 2. This reflects the sensitivity enhancement achieved by the addition of the phase-inverted HH-CP. Furthermore, the PILGRIM time signal is mostly negative and approaches a final value close to 0 (with a slight offset), while the LG-CP time signal is mostly positive and approaches an equilibrium value that is half the maximum amplitude. These time-domain features are consistent with eqs 7 and 10. Again, the intensity offsets in the time oscillations are corrected before the Fourier transformation and do not influence the final frequency spectra.

Interestingly, when the PILGRIM experiment was carried out on a ^{13}C natural abundance sample of *N*-acetylvaline, the Cα signal was not enhanced further, as one might expect for a sample with an overall larger spin number ratio between ^{1}H and ^{13}C. This indicates that ^{1}H spin diffusion during HH-CP is very inefficient at the relatively fast spinning speed of 13 kHz.[22] In other words, cross polarization only connects spins that are within two and three bonds of each other. This is consistent with calculations by Vega and co-workers for spinning speeds between 10 and 20 kHz, which showed that the CP signal of an *S* spin in an environment of six protons has an ϵ of 0.6−0.75 [22] rather than the theoretical value of 0.86.

^{13}C-Detected $^{15}N-^{1}H$ LG-CP Spectroscopy. Figure 10 shows the N−H LG-CP line shape of the side chain NH_2 of U-^{13}C,^{15}N-labeled glutamine, obtained with ^{15}N direct detection (Figure 10a) and ^{13}C indirect detection (Figure 10b). The ^{13}C detected spectrum was extracted from the Cδ cross section of the 2D spectrum. The two detection schemes yielded identical splittings and very similar line shapes, except that the outer shoulders in the ^{13}C-detected spectrum are slightly broadened. The central intensities in the ^{13}C detected spectrum (Figure 10b) probably result from the backbone NH_3 group, due to long-range correlation between the side chain Cδ and the backbone

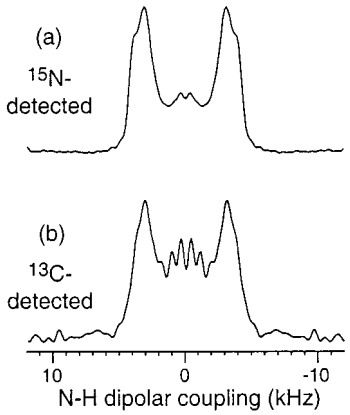

Figure 10. $^{15}N-^{1}H$ LG-CP spectrum of side chain NH_2 in glutamine: (a) ^{15}N directly detected spectrum, (b) ^{13}C indirectly detected spectrum.

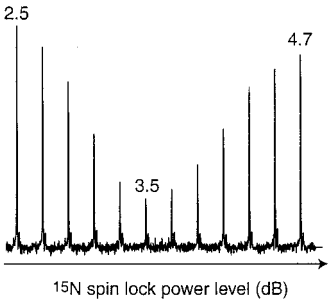

Figure 11. Dependence of NH_2 peak intensities of glutamine on the ^{15}N power level during the $^{1}H-^{15}N$ contact time in the ^{13}C-detected N−H LG-CP experiment. The minimum peak intensity corresponds to the optimum ^{15}N spin-lock field that matches the ^{1}H spin-lock field strength.

^{15}N during the REDOR periods. The backbone NH_3 spectrum (not shown) exhibited no clear splitting by either method, consistent with the fast three-site jump motion.

To set up this indirectly ^{13}C-detected $^{15}N-^{1}H$ LG-CP experiment, we need to determine the optimal sideband matching condition for ^{15}N and ^{1}H spin-lock. This is achieved empirically by choosing the contact time that corresponds to the first trough in the N−H dipolar oscillation curve, then fixing the ^{1}H spin-lock field strength, and varying the ^{15}N power level until the peak intensity reaches a minimum. Figure 11 shows a series of NH_2 signal heights as a function of the ^{15}N power

level during $^{15}N-^{1}H$ LG-CP at 0.2 dB increments. The CP contact time used was 153.8 μs, which corresponded to two rotation periods. A clear global minimum is observed at a ^{15}N power level of 3.7 dB. This value was then used in the final experiment.

5. Conclusion

We have demonstrated that the LG-CP technique can be used to investigate local segmental motions in both small organic molecules and macromolecules. The LG-CP evolution yields simple and well-resolved splittings in the frequency domain, whose line shape can be analyzed to extract semiquantitative information on the geometry of motion. Application to phenylalanine indicates that fast 180° ring flips with a reorientation angle of 124° describe the phenylene dynamics reasonably well. In comparison, the LG-CP spectra of the phenylene rings in polycarbonate agree with a motional model that combines 180° ring flips with small-amplitude wobbling with a 20° distribution of the wobbling amplitudes.

Combining the C−H and N−H dipolar coupling measurements by LG-CP, we can now better define the motional mechanisms of the membrane-bound colicin Ia channel domain. Since the N−H narrowing factors between the membrane-bound protein and the soluble protein are nearly identical to the Cα−Hα narrowing factors, we suggest that the backbone motions in the membrane-bound colicin may be wobbling motions of each residue or helix. Specifically, we can rule out reorientation around the helix axes as a motional mechanism. The N-terminal His tag exhibits larger amplitude motions, suggesting that it is a random coil unassociated with the lipid bilayer.

The addition of a phase-inverted HH-CP step before LG-CP evolution increased the sensitivity of the LG-CP dipolar spectra by a factor of 1.3−1.6 in amino acids. The enhancement factor can be understood from the ratio of the ^{1}H spins to ^{13}C spins in the local environment of the ^{13}C spins of interest. ^{13}C indirect detection of the N−H LG-CP spectra increases the site resolution of the LG-CP dipolar couplings. Demonstration on glutamine shows that the dipolar coupling information is retained faithfully.

We expect the LG-CP experiment to be particularly useful for studying the dynamics of isotopically labeled biological macromolecules, where the use of high magnetic fields require high MAS speeds, making the traditional DIPSHIFT experiment inapplicable.

Acknowledgment. This work is supported by a NSF CAREER award (MCB-0093398) and a Beckman Young Investigator Award to M.H. The authors thank Prof. Schmidt-Rohr for helpful discussions on polycarbonate dynamics, and one reviewer for constructive comments on the LG-CP spin dynamics. D.H. is grateful for a postdoctoral fellowship from the BASF AG and the Studienstiftung des deutschen Volkes.

References and Notes

(1) Palmer, A. G.; Williams, J.; McDermott, A. *J. Phys. Chem.* **1999**, *100*, 13293.
(2) Spiess, H. W. *Adv. Polym. Sci.* **1985**, *66*, 23.
(3) Schmidt-Rohr, K.; Clauss, J.; Spiess, H. W. *Macromolecules* **1992**, *25*, 3273.
(4) Clauss, J.; Schmidt-Rohr, K.; Spiess, H. W. *Acta Polym.* **1993**, *44*, 1.
(5) Munowitz, M. G.; Griffin, R. G.; Bodenhausen, G.; Huang, T. H. *J. Am. Chem. Soc.* **1981**, *103*, 2529.
(6) Munowitz, M.; Aue, W. P.; Griffin, R. G. *J. Chem. Phys.* **1982**, *77*, 1686.
(7) Schaefer, J.; Stejskal, E. O.; Perchak, D.; Skolnick, J.; Yaris, R. *Macromolecules* **1985**, *18*, 368.
(8) Huster, D.; Xiao, L. S.; Hong, M. *Biochemistry* **2001**, *40*, 7662.
(9) Schaefer, J.; Stejskal, E. O.; Mckay, R. A.; Dixon, W. T. *Macromolecules* **1984**, *17*, 1479.
(10) Lee, M.; Goldburg, W. I. *Phys. Rev.* **1965**, *140*, A1261.
(11) vanRossum, B. J.; deGroot, C. P.; Ladizhansky, V.; Vega, S.; deGroot, H. J. M. *J. Am. Chem. Soc.* **2000**, *122*, 3465.
(12) Ladizhansky, V.; Vega, S. *J. Chem. Phys.* **2000**, *112*, 7158.
(13) Nielsen, N. C.; Bildsoe, H.; Jakobsen, H. J.; Levitt, M. H. *J. Chem. Phys.* **1994**, *101*, 1805.
(14) Lee, Y. K.; Kurur, N. D.; Helmle, M.; Johannessen, O. G.; Nielsen, N. C.; Levitt, M. H. *Chem. Phys. Lett.* **1995**, *242*, 304.
(15) Huster, D.; Yamaguchi, S.; Hong, M. *J. Am. Chem. Soc.* **2000**, *122*, 11320.
(16) Hong, M.; Jakes, K. *J. Biomol. NMR* **1999**, *14*, 71.
(17) Bennett, A. E.; Rienstra, C. M.; Auger, M.; Lakshmi, K. V.; Griffin, R. G. *J. Chem. Phys.* **1995**, *103*, 6951.
(18) Schmidt-Rohr, K.; Spiess, H. W. *Multidimensional Solid-State NMR and Polymers*, 1st; Academic Press: San Diego, 1994.
(19) Haeberlen, U. *High-Resolution NMR in Solids: Selective Averaging*, Academic Press: 1976.
(20) Wu, C. H.; Ramamoorthy, A.; Opella, S. J. *J. Magn. Reson. Ser A* **1994**, *109*, 270.
(21) Ramamoorthy, A.; Wu, C. H.; Opella, S. J. *J. Magn. Reson.* **1999**, *140*, 131.
(22) Ray, S.; Ladizhansky, V.; Vega, S. *J. Magn. Reson.* **1998**, *135*, 427.
(23) Gan, Z. *J. Magn. Reson.* **2000**, *143*, 136.
(24) Bodenhausen, G.; Ruben, D. J. *Chem. Phys. Lett.* **1980**, *69*, 185.
(25) Wehrle, M.; Hellmann, G. P.; Spiess, H. W. *Colloid Polym. Sci.* **1987**, *265*, 815.
(26) Frey, M. H.; DiVerdi, J. A.; Opella, S. J. *J. Am. Chem. Soc.* **1985**, *107*, 7311.
(27) Mowery, D.; Harris, D.; Schmidt-Rohr, K. Manuscript in preparation.
(28) Hansen, M. T.; Blumich, B.; Boeffel, C.; Spiess, H. W.; Morbitzer, L.; Zembrod, A. *Macromolecules* **1992**, *25*, 5542.
(29) Cramer, W. A.; Heymann, J. B.; Schendel, S. L.; Deriy, B. N.; Cohen, F. S.; Elkins, P. A.; Stauffacher, C. V. *Annu. Rev. Biophys. Biomol. Struct.* **1995**, *24*, 611.
(30) Wiener, M.; Freymann, D.; Ghosh, P.; Stroud, R. M. *Nature* **1997**, *385*, 461.
(31) Hong, M. *J. Magn. Reson.* **1999**, *136*, 86.
(32) Hong, M. *J. Biomol. NMR* **1999**, *15*, 1.
(33) Huster, D.; Yao, X. L.; Hong, M. *J. Am. Chem. Soc.* **2002**, *124*, 874.
(34) Lindeberg, M.; Zakharov, S. D.; Cramer, W. A. *J. Mol. Biol.* **2000**, *295*, 679.
(35) Huster, D.; Yao, X.; Jakes, K.; Hong, M. *Biochim. Biophys. Acta* **2002**, in press.
(36) Farrens, D. L.; Altenbach, C.; Yang, K.; Hubbell, W. L.; Khorana, H. G. *Science* **1996**, *274*, 768.
(37) Perozo, E.; Cortes, D. M.; Cuello, L. G. *Science* **1999**, *285*, 73.
(38) Usha, M. G.; Peticolas, W. L.; Wittebort, R. J. *Biochemistry* **1991**, *30*, 3955.